

# Eliminating Dispersion Power Fading in Radio over Fiber Communication through Unbalanced Sideband Modulation

Febrizal Ujang<sup>1,\*</sup>, Anhar<sup>1</sup>, Esra Erianti Butar Butar<sup>1</sup>, Silvia Anggraeni<sup>2</sup>, Syah Alam<sup>3</sup>, Ken Paramayudha<sup>4</sup>, Rocky Alfan<sup>5</sup>, and Teguh Firmansyah<sup>5</sup>

<sup>1</sup> Department of Electrical Engineering, Universitas Riau, Pekanbaru, Indonesia

<sup>2</sup> Department of Electrical Engineering, Universitas Pembangunan Nasional Veteran Jakarta, Jakarta, Indonesia

<sup>3</sup> Department of Electrical Engineering, Universitas Trisakti, Jakarta, Indonesia

<sup>4</sup> Research Center for Telecommunication, National Research and Innovation Agency (BRIN), Bandung, Indonesia

<sup>5</sup> Department of Electrical Engineering, Universitas Sultan Ageng Tirtayasa, Cilegon, Indonesia

Email: febrizal@eng.unri.ac.id (F.U.), anhar@lecturer.unri.ac.id (A.), esra.erianti4872@student.unri.ac.id (E.E.B.B.), silvia.anggraeni@upnvj.ac.id (S.A.), syah.alam@trisakti.ac.id (S.A.), ken.paramayudha@brin.go.id (K.P.), rocky.alfanz@untirta.ac.id (R.A.), teguhfirmansyah@untirta.ac.id (T.F.)

**Abstract**—In Radio Over Fiber (RoF) systems, a commonly used approach to reduce the Dispersion Power Fading (DPF) effects is to convert the spectrum of modulated optical signals into Optical Single Sideband (OSSB). This process can be done by modulating the optical carrier using two RF signals that differ in phase by  $90^\circ$ . The optical modulator used is the Dual-Drive Mach Zehnder Modulator (DD-MZM). However, implementing this modulation scheme requires a complex transmitter setup. In this study, a novel technique is proposed to address DPF, called as Unbalanced Sideband Modulation (USM). USM is generated by varying the optical signal carrier according to the RF signal using a Single-Drive Mach Zehnder Modulator (SD-MZM). The output of the SD-MZM is subsequently combined with an optical signal of a frequency equivalent to the sum of the optical carrier frequency and the Radio Frequency (RF) signal frequency. The result outcomes indicate that at a modulation index ( $m$ ) of 1, the DPF level in a RoF link employing conventional SD-MZM as an Electro-Optic (E/O) converter is approximately 8.2. In contrast, when using the OSSB produced by the DD-MZM, the DPF level of a RoF link is around 0.9. Remarkably, the DPF level significantly drops to 0.2 when the USM scheme is adopted. This result shows the high efficacy of the USM scheme in eliminating DPF compared to both the conventional SD-MZM modulation scheme and the OSSB scheme generated by DD-MZM. Both model calculations and numerical simulations conclusively demonstrate that the USM method effectively mitigates DPF, offering a promising solution in optical communication systems.

**Keywords**—Dispersion power fading, radio over fiber, Single-Drive Mach Zehnder Modulator (SD-MZM), unbalance sideband modulation

## I. INTRODUCTION

Currently, the development and research of systems capable of transmitting Radio Frequency (RF) signals via optical fibers have made significant progress. These

systems are used to utilized mobile communication system known as Radio Over Fiber (RoF). Optical signals are modulated by RF signals using Electro-Optic (E/O) converters in the process of transmitting signals from the Central Office (CO) to the Radio Access Point (RAP). This modulated optical signal is then at the Radio Access Point (RAP) converted back into an RF signal using an Opto-Electric (O/E) converter. Then, the output RF signal of the E/O converter is transmitted over the air from the RAP to the user's Mobile Station (MS). The E/O process can be done through direct modulation or externally. Both modulation techniques can produce intensity modulation (amplitude) as well as phase modulation. RF signal recovery in Intensity Modulation (IM) techniques is commonly known as Direct Detection (DD), while in the case of phase modulation, it is known as Coherent Detection (CD) [1–3].

When an RF signal modulates an optical signal with the IM technique, it will produce an optical signal with an Optical Double Sideband (ODSB) shaped spectrum. This spectrum encompasses components such as the optical carrier, upper sidebands, and lower sidebands [4–7].

When an ODSB signal is passed into an optical fiber, the optical carrier and sideband components will propagate at different velocity. This happens due to the chromatic dispersion of the fiber. The velocity difference of these two components also causes a phase difference by  $\phi$ . The value of  $\phi$  is affected by factors such as fiber length ( $L$ ), RF signal frequency ( $f_m$ ), and wavelength ( $\lambda_c$ ). The existence of  $\phi$  triggers the formation of two RF signals in the opto-electronic (O/E) conversion process that have the same magnitude but differ in phase by  $2\phi$ . As a result, constructive and destructive interference appears within the generated RF signal. A decrease in power in the generated signal occurs when destructive interference occurs, a phenomenon known as Dispersion Power Fading (DPF). To make matters worse, when  $\phi = \pi/2$ , the

Manuscript received June 20 2024; revised July 26 2024, accepted August 6 2024.

\*Corresponding author

generated signal power will be equal to zero. The condition when this occurs is referred to as deep fade [8].

One of the techniques employed to mitigate DPF is the Carrier Phase Shifted (CPS) techniques [9]. In these techniques, the phase of optical carrier ( $\phi$ ) is preconfigured at transmitter, ensuring that  $\phi$  becomes zero after transmission. Through this approach, the recovered RF signal consistently maintains a constructive condition. However, a limitation of this method is that the  $\phi$ , needs to be consistently re-adjusted to match the specific parameters of  $L$ ,  $f_m$ , and  $\lambda_c$ . This adjustment is necessary because the proportion of  $\phi$  is contingent upon  $L$ ,  $f_m$ , and  $\lambda_c$  values. Therefore, this method is not convenience and lacks robustness.

Furthermore, another approach to reduce DPF involves transforming the shape of the modulated optical signal spectrum into Optical Carrier Suppressed (OCS) format [10–14]. OCS modulation is generated by suppressing the optical carrier component of the ODSB signal so that the signal consists of only the lower and upper sidebands. With this technique, the photodetector generates only one RF signal which is the multiplication of the lower and upper sidebands thus effectively avoiding DPF. However, the drawback of this technique is that the resulting RF signal frequency is double the original RF signal frequency. Therefore, a down conversion process is required at the receiver to restore the original frequency.

The DPF can also be effectively addressed using the Optical Single Sideband (OSSB) modulation scheme [5, 13, 15–21]. The OSSB modulation generates a spectrum that included only one of the sidebands (upper or lower) and the optical carrier. With OSSB modulation, a single recovered RF signal is generated, having the same frequency as the transmitted RF signal. As a result, the receiver does not require a down-conversion processes. OSSB can be generated from a Dual Drive Mach-Zehnder Modulator (DD-MZM) biased at the Quadrature Bias Point (QBP) and given two RF signal inputs having a phase difference of  $\pi/2$  [22–27]. It's important to note that generating OSSB modulation using this approach requires a complex transmitter circuitry due to the required phase adjustment and biasing configuration. To address these challenges, this research introduces the Unbalanced Sideband Modulation (USM) method. Several contributions from this study are outlined below:

- 1) The proposed USM scheme, implemented using SD-MZM, demonstrates significantly greater effectiveness compared to both the conventional SD-MZM and the OSSB scheme generated by DD-MZM.
- 2) Furthermore, the USM scheme can be achieved by combining a conventional SD-MZM with an additional optical signal and a combiner. This simple adaptability enables its integration into existing fiber optic networks utilizing conventional SD-MZMs.
- 3) The application of the USM method does not require adjustments to parameters such as fiber length ( $L$ ), RF signal frequency ( $f_m$ ), and wavelength ( $\lambda_c$ ). Consequently, the obtained results exhibit enhanced stability and robustness.
- 4) Both calculated and simulated results show the

remarkable effectiveness of the USM scheme in eliminating DPF when compared to both the conventional SD-MZM scheme and the OSSB scheme generated by the DD-MZM. These comprehensive analyses conclusively establish the USM methods capability to effectively counteract DPF, thereby offering a promising avenue for enhancing optical communication systems.

Moreover, it should be noted, as the limitation of this study, the laser powers used in this research (0 dBm, 5 dBm, and 10 dBm) are only for the samples. This aims to prove the hypothesis that the greater the difference in power between USB and LSB, the more effective USM is in overcoming DPF. From the results of calculations and simulations, it is shown that only laser powers of 5 dBm and 10 dBm can overcome DPF better than OSSB. This means that for LD<sub>2</sub> power greater than 10 dBm, USM performance will be better than OSSB, whereas if the laser power is smaller than 5 dBm, USM performance will be increasingly reduced. This is because the smaller the difference in USB power compared to LSB, the smaller the difference in the resulting RF<sub>1</sub> and RF<sub>2</sub> signal power will be. The lesser the magnitude of the difference, the greater the interference encountered.

## II. SINGLE DRIVE MACH ZEHNDER MODULATOR (SD-MZM)

### A. Principle of SD-MZM

The SD-MZM represents a commonly used external optical modulator in the field of optical communication. The fundamental architecture of the Mach-Zehnder Modulator (MZM) consists of two arms, as depicted in Fig. 1. The incident optical signal is split into these two arms. The MZM can be actuated (driven) along one or both of these two arms. Specifically, when modulation is applied to a single arm, it is denoted as a SD-MZM. Output of the SD-MZM, which receive the optical input signal  $E_{in}(t) = E_o e^{j2\pi f_c t}$  originating from a laser diode (LD) and driven by the electrical signal  $X_{TX}(t)$ , while under the influence of a bias voltage  $V_{bias}$ , is mathematically expressed as detailed in reference [28].

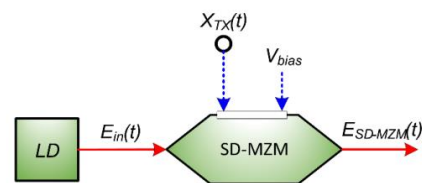


Fig. 1. The structure of SD-MZM.

$$E_{SD-MZM}(t) = \frac{1}{2} E_o e^{j2\pi f_c t} \left[ e^{j\pi \left( \frac{X_{TX}(t) + V_{bias}}{V_\pi} \right)} + 1 \right] \quad (1)$$

where  $E_o$  and  $f_c$  represents the amplitude and optical frequency, respectively. Additionally,  $V_\pi$  denotes the MZM switching voltage.

If  $X_{TX}(t)$  represents an RF signal, it can be calculated as

$$X_{TX}(t) = V_m \cos 2\pi f_m t, \quad (2)$$

where  $f_m$  and  $V_m$  is the frequency and RF signal amplitude respectively. Therefore, (1) can be expressed as

$$E_{SD-MZM}(t) = \frac{1}{2} E_o e^{j2\pi f_c t} \left\{ e^{j\pi \frac{V_m}{V_\pi} \cos(2\pi f_m t) + j\pi \frac{V_{bias}}{V_\pi}} + 1 \right\} \quad (3)$$

Eq. (3) can be further simplified as:

$$\begin{aligned} E_{SD-MZM}(t) &= \frac{1}{2} E_o e^{j2\pi f_c t} \{ e^{jm \cos(2\pi f_m t) + j\pi\gamma} + 1 \} \\ &= \frac{1}{2} E_o e^{j2\pi f_c t} \{ e^{jm \cos(2\pi f_m t)} \cdot e^{j\pi\gamma} + 1 \} \end{aligned} \quad (4)$$

where  $m = \pi V_m / V_\pi$  is the modulation index of SD-MZM, and  $\gamma = V_{bias} / V_\pi$  is the bias voltage of normalized. For easy analysis, Eq. (4) can be derived as:

$$E_{SD-MZM}(t) = \frac{1}{2} E_o e^{j2\pi f_c t} \{ A e^{j\pi\gamma} + 1 \} \quad (5)$$

where

$$A = e^{jm \cos(2\pi f_m t)} \quad (6)$$

By utilizing a Jacobi Anger expansion [29], where

$$e^{jm \cos x} = \sum_{n=-\infty}^{\infty} j^n J_n(m) e^{jnx} \quad (7)$$

$$e^{jm \sin x} = \sum_{n=-\infty}^{\infty} J_n(m) e^{jnx} \quad (8)$$

So, Eq. (6) becomes

$$A = \sum_{n=-\infty}^{\infty} j^n J_n(m) e^{jn(2\pi f_m t)} \quad (9)$$

where  $J_n(m)$  is a Bessel function the  $n$ th order. Therefore, Eq. (4) can be determined by

$$\begin{aligned} E_{SD-MZM}(t) &= \frac{1}{2} E_o e^{j2\pi f_c t} \left\{ \sum_{n=-\infty}^{\infty} j^n J_n(m) (e^{jn(2\pi f_m t)} \cdot e^{j\pi\gamma} + 1) \right\} \\ &= \frac{1}{2} E_o \{ e^{j2\pi f_c t} + \sum_{n=-\infty}^{\infty} e^{j\pi\gamma} j^n J_n(m) e^{j2\pi(f_c + n f_m)t} \} \end{aligned} \quad (10)$$

Eq. (10) indicates that the output of the SD-MZM is an optical field consisting of optical carriers and infinite order sidebands. The SD-MZM output has a double sideband (ODSB) spectrum, as can be seen in Fig. 2. The lower and upper sideband of each order have the same magnitude. According to the function of Bessel, the sideband formation orders is determined by the  $m$  value. Specifically, larger values of  $m$  result in the formation of more sideband orders.

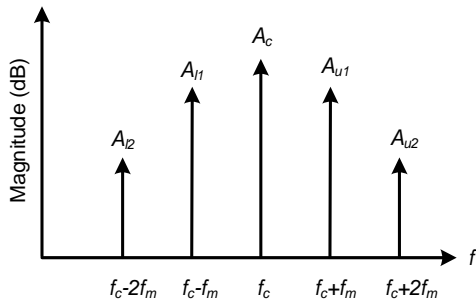


Fig. 2. The structure of SD-MZM.

## B. Dispersion Power Fading

Dispersion power fading (DPF) on link RoF can be observed through curve of the C/N penalty, while the DPF level can be measured by calculating the standard deviation of the C/N penalty [30]. The C/N penalty represents the reduction proportion in the generated RF signal power over a fiber length  $L$  ( $P_{rec}(L)$ ) due to fiber dispersion. The C/N penalty is obtained from comparison with and without fiber of the  $P_{rec}(L)$ . This can be expressed as [8]

$$\frac{C}{N} \text{ penalty} = 10 \log \left| \frac{P_{rec}(L)_{\text{with fiber}}}{P_{rec}(L)_{\text{without fiber}}} \right| \quad (11)$$

$P_{rec}(L)$  equation needs to be derived in order to calculate the C/N penalty of the RoF channel with SD-MZM. The model of this channel can be seen in Fig. 3. This channel is composed of an E/O converter (using SD-MZM), an optical fiber with response of  $H(f)$ , and an O/E converter (using a photodetector (PD)).

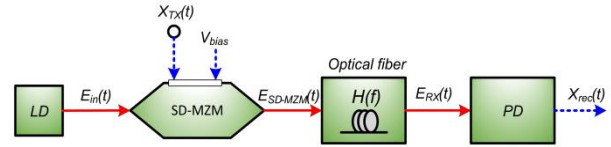


Fig. 3. RoF link with SD-MZM as E/O converter.

To simplify the analysis, Eq. (10) is rewritten as

$$\begin{aligned} E_{SD-MZM}(t) &= A_c e^{j2\pi f_c t} + \\ &\sum_{n=1}^{\infty} \{ A_{ln} e^{j2\pi(f_c - n f_m)t} + A_{un} e^{j2\pi(f_c + n f_m)t} \} \end{aligned} \quad (12)$$

where:

$$A_c = \frac{1}{2} E_o \{ 1 + e^{j\pi\gamma} J_0(m) \}$$

$$A_{ln} = A_{un} = \frac{1}{2} E_o e^{j\pi\gamma} j^n J_n(m)$$

The dispersive fiber channel transfer function is given by [31]:

$$H(f) = e^{\frac{j\pi D L \lambda_c^2 (f - f_c)^2}{c}} \quad (13)$$

where  $D$ ,  $c$ ,  $L$ ,  $\lambda_c$ , and  $f$  are the chromatic dispersion (ps/(nm.km)), speed of light in vacuum, fiber length, wavelength, and frequency offset of the optical carrier, respectively. While  $E_{SD-MZM}(t)$  enters the dispersive channel, a phase difference  $\phi$  appears among the optical carrier and the first-order sideband.

$$\phi = \frac{\pi D L \lambda_c^2 f_m^2}{c}, \quad (14)$$

while the  $\phi$  is the distance of frequency square ( $\pm n f_m$ ) given by [32]

$$\phi_n = n^2 \phi \quad (15)$$

so, at the receiver will arrive an optical field ( $E_{RX}(t)$ ) has the form:

$$\begin{aligned} E_{RX}(t) &= A_c e^{j2\pi f_c t} + \\ &\sum_{n=1}^{\infty} \{ A_{ln} e^{j2\pi(f_c - n f_m)t} + A_{un} e^{j2\pi(f_c + n f_m)t} \} e^{jn^2 \phi} \end{aligned} \quad (16)$$

Detecting process of  $E_{RX}(t)$  at the receiver using photodetector is the squared envelope operator given by [8]

$$|E_{RX}(t)|^2 = E_{RX}(t)E_{RX}^*(t) \quad (17)$$

By taking the term  $f_m$ , it is obtained:

$$\begin{aligned} |E_{RX}(t)|^2 &= e^{j2\pi f_m t} \{ A_c A_{l1}^* e^{-j\phi} + A_c^* A_{u1} e^{j\phi} \\ &\quad + A_{l1} A_{l2}^* e^{-j3\phi} + A_{u1}^* A_{u2} e^{j3\phi} \\ &\quad + A_{l2} A_{l3}^* e^{-j5\phi} + A_{u2}^* A_{u3} e^{j5\phi} + \dots \} \\ &= e^{j2\pi f_m t} \{ \sum_{n=0}^{\infty} A_{ln} A_{l(n+1)}^* e^{-j(2n+1)\phi} + \\ &\quad A_{un}^* A_{u(n+1)} e^{j(2n+1)\phi} \} \end{aligned} \quad (18)$$

where  $A_{l0} = A_{u0} = A_c$ .

The real part of Eq. (18) is equal to the power of the photodetector ( $X_{rec}(t)$ ) [31], therefore:

$$X_{rec}(t) \approx \left\{ \sum_{n=0}^{\infty} A_{ln} A_{l(n+1)}^* e^{-j(2n+1)\phi} + A_{un}^* A_{u(n+1)} e^{j(2n+1)\phi} \right\} \cos 2\pi f_m t \quad (19)$$

The power of  $X_{rec}(t)$  is obtained by squaring the amplitude term from Eq. (19) [8], so that the power of generated RF signal as a function of  $L$  is stated by:

$$P_{rec}(L) = \left\{ \sum_{n=0}^{\infty} A_{ln} A_{l(n+1)}^* e^{-j(2n+1)\phi} + A_{un}^* A_{u(n+1)} e^{j(2n+1)\phi} \right\}^2 \quad (20)$$

where:

$$\begin{aligned} \phi &= \frac{\pi D L \lambda_c^2 f_m^2}{c} \\ A_c &= \frac{1}{2} E_o \{ 1 + e^{j\pi\gamma} J_0(m) \} \\ A_{ln} &= A_{un} = \frac{1}{2} E_o e^{j\pi\gamma} j^n J_n(m) \\ A_c^* &= \frac{1}{2} E_o \left( 1 + e^{-j\pi\gamma} J_n(m) \right) \\ A_{ln}^* &= A_{un}^* = \frac{1}{2} E_o e^{-j\pi\gamma} (-j^n) J_n(m). \end{aligned}$$

The RF signal results from multiplying the  $n$ th-order lower sideband by the conjugate of order  $(n+1)$ , plus multiplying the conjugate of the  $n$ th-order upper sideband by order  $(n+1)$ . Here,  $n$  is an integer. Furthermore, the RF signal power is calculated by squaring the amplitude of the RF signal.

The DPF of the RoF channel with SD-MZM was observed using the C/N penalty curve calculated using (11), where  $P_{rec}(L)$  is determined using (20). For this calculation, the SD-MZM is biased at the quadrature bias point (QBP) with  $\gamma = 1/2$ . The optical wavelength used ( $\lambda_c$ ) = 1550 nm, the optical signal amplitude ( $E_o$ ) = 0.045 V or equivalent to the laser power ( $P_o$ ) = 0 dBm (assuming impedance  $Z = 1 \Omega$ ). The dispersion coefficient ( $D$ ) for this wavelength is 17 ps/nm.km. The RF signal frequency ( $f_m$ ) employed is 60 GHz. Fiber length range ( $L$ ) is chosen from 0 km to 5 km with an interval of 0.1 km. The modulation index ( $m$ ) in this calculation is set to 0.1, 0.5, 0.8, and 1. The calculated C/N penalty curve for the RoF channel with SD-MZM is shown in Fig. 4.

In Fig. 4, the vertical and horizontal axes represent the C/N penalty (dB) and fiber length (km), respectively. The curve shows that power fluctuations occur in the produced RF signal across all  $m$ , and deep fade are consistently observed at approximately the same points:  $L = 1.5$  km and

$L = 3.5$  km. This means the presence of persistent DPF in the RoF channel with SD-MZM. Remarkably, deep fade consistently emerges at similar fiber lengths for different  $m$ . The DPF levels for this RoF link, corresponding to  $m$  of 0.1, 0.5, 0.8 and 1, are measured as 6.6, 6.9, 8.9 and 8.2 dB, respectively. This clearly shows substantial fluctuation in the generated RF power signal within the RoF channel using SD-MZM.

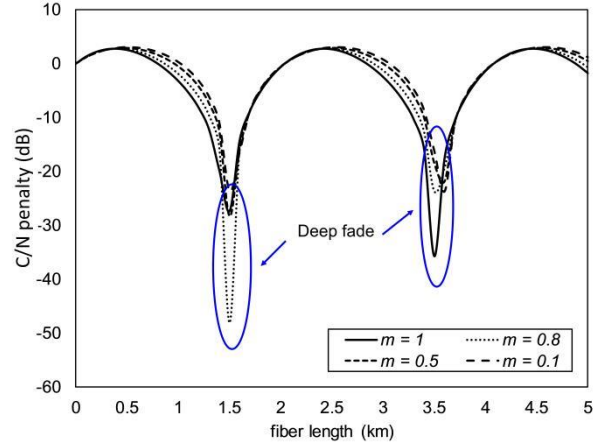


Fig. 4. C/N penalty from RoF link with SD-MZM as E/O converter.

### III. UNBALANCE SIDEBAND MODULATION

#### A. Principle of Unbalance Sideband Modulation

The occurrence of DPF on the RoF link can be explained through the evolution of the optical spectrum in Fig. 5 (a) – Fig. 5 (c). Optical signal modulation by RF signals using SD-MZM produces a spectrum with a Double Sideband (DSB) shape, as shown in Fig. 5 (a). When the DSB signal propagates over a dispersive link, each spectral component will traverse the medium at a different speed. This variance in speed leads a relative phase difference among the two sidebands and the Optical Carrier (OC), illustrated in Fig. 5 (b). When this signal is detected using a PD, two RF signals are generated, as shown in Fig. 5 (c). The RF I signal originates from the beating between the OC and the Lower Sideband (LSB), while the RF II signal is formed from the beating between the OC and the Upper Sideband (USB). These two signals have the same magnitude but differ in phase by  $2\phi$ . Because the value of  $\phi$  is influenced by the length of the fiber ( $L$ ), then constructive and destructive interference (known as DPF) will occur as  $L$  changes. When the  $\phi$  value reaches  $\pi/2$ , the two RF signals counteract each other resulting in a substantial drop in RF signal power, which is known as a deep fade.

In this paper, we propose an Unbalanced Sideband Modulation (USM) method to overcome DPF. USM is an optical modulation scheme characterized by a spectrum configuration, as shown in Fig. 5 (d). In this scheme, the magnitude of USB is intentionally rendered greater than that of the OC and the LSB. When the USM signal propagates through the dispersive channel, a relative phase difference among the two sidebands and the OC arises, illustrated in Fig. 5 (e). When this signal is detected using a PD, two RF signals that differ in phase by  $2\phi$  will be

generated. These two signals also have different magnitudes as shown in Fig. 5 (f). Because these two signals have different magnitudes, the interference

originating from these two signals is mitigated. The greater the magnitude difference, the lesser the interference encountered.

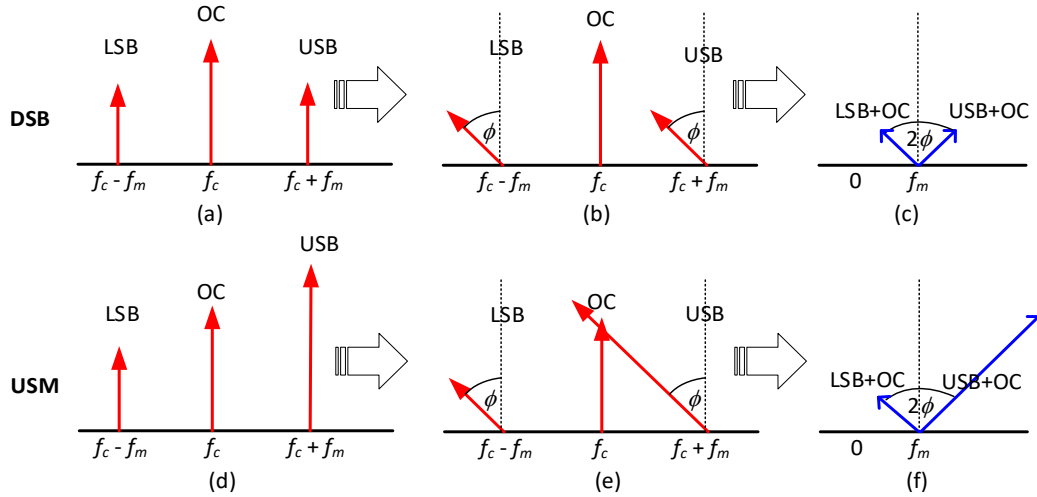


Fig. 5. Optical signal evolution along the RoF link: (a) – (c) with SD-MZM as E/O converter [conventional], (d) – (f) with USM [proposed].

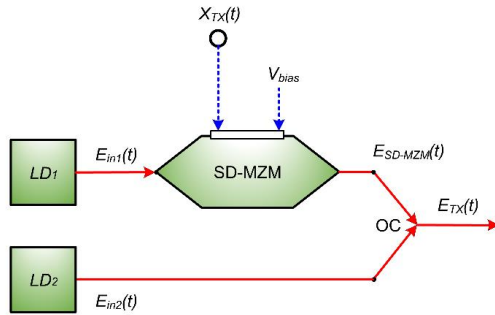


Fig. 6. Proposed of schematic of USM modulator.

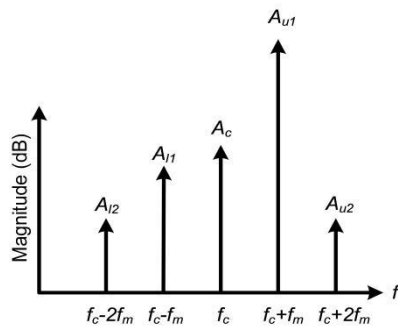


Fig. 7. Optical spectrum of USM [proposed].

USM can be generated using a circuit like in Fig. 6. The SD-MZM output is combined with the LD<sub>2</sub> output, which has a frequency of  $f_c + f_m$ . LD<sub>1</sub> generates an optical carrier signal represented by  $E_{in1}(t) = E_{o1}e^{j2\pi f_c t}$  which modulated by an RF signal that has a frequency of  $f_m$  using SD-MZM. This modulated signal is subjected to a bias voltage of  $V_{bias}$ . The SD-MZM output and the optical signal generated by LD<sub>2</sub> are then combined using an optical combiner (OC). The optical signal generated by LD<sub>2</sub> is expressed by  $E_{in2}(t) = E_{o2}e^{j2\pi(f_c + f_m)t}$ , where  $E_{o1}$  and  $E_{o2}$  denote the optical signal amplitudes of LD<sub>1</sub> and LD<sub>2</sub>, respectively.

The output optical field of the USM modulator ( $E_{TX}(t)$ )

results from the addition of  $E_{SD-MZM}(t)$  and  $E_{in2}(t)$ . This can be expressed as follows:

$$E_{TX}(t) = E_{SD-MZM}(t) + E_{in2}(t)$$

$$= \frac{1}{2}E_{o1} \left\{ e^{j2\pi f_c t} + \sum_{n=-\infty}^{\infty} e^{j\pi \gamma} j^n J_n(m) e^{j2\pi(f_c + n f_m)t} \right\} + E_{o2}e^{j2\pi(f_c + f_m)t} \quad (21)$$

From Eq. (21) it can be seen that USB I of the USM optical field exhibits a larger amplitude compared to the LSB I. Moreover, the amplitudes of USB and LSB for other orders remain uniform. The shape of the output spectrum of the USM modulator can be seen in Fig. 7.

### B. USM's Performance in Mitigating DPF

$P_{rec}(L)$  equation needs to be derived to see the performance of USM in mitigating DPF on the RoF channel. The RoF channel model with USM is shown in Fig. 8. The RoF channel is composed of a transmitter, link and a receiver. The transmitter is composed of an SD-MZM, LD<sub>1</sub> as an optical carrier generator, and LD<sub>2</sub> as an injector for an upper sideband order I. The link in this model is a dispersive fiber optic channel with the response of  $H(f)$ . On the other hand, the receiver consists of photodetector (PD) which functions as an O/E converter.

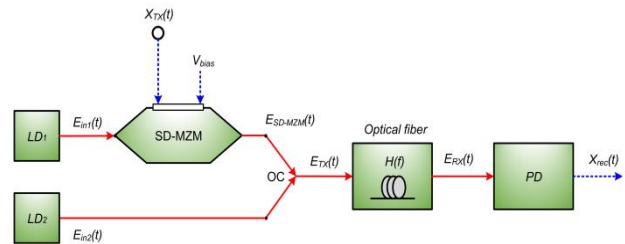


Fig. 8. RoF link with unbalance sideband modulator [proposed].

For ease of analysis, (21) can be arranged to mirror (12), yielding

$$E_{TX}(t) = A_c e^{j2\pi f_c t} + \sum_{n=1}^{\infty} \{A_{ln} e^{j2\pi(f_c - n f_m)t} + A_{un} e^{j2\pi(f_c + n f_m)t}\} \quad (22)$$

with values of  $A_c$ ,  $A_{ln}$  and  $A_{un}$  is equal to the values in (12). Additionally, the value of  $A_{u1}$  can be expressed as  $\frac{1}{2}E_{o1} e^{j\pi\gamma} j J_1(m) + E_{o2}$ . Because (22) has the same form as (12), the equation for the recovered RF signal for this RoF link ( $X_{rec}(t)$ ) also retains the same structure as (19):

$$X_{rec}(t) \approx \left\{ \sum_{n=0}^{\infty} A_{ln} A_{l(n+1)}^* e^{-j(2n+1)\phi} + A_{un}^* A_{u(n+1)} e^{j(2n+1)\phi} \right\} \cos 2\pi f_m t \quad (23)$$

Furthermore, the recovered RF signal power for this RoF link ( $P_{rec}(L)$ ) maintains the same form to (20):

$$P_{rec}(L) = \left\{ \sum_{n=0}^{\infty} A_{ln} A_{l(n+1)}^* e^{-j(2n+1)\phi} + A_{un}^* A_{u(n+1)} e^{j(2n+1)\phi} \right\}^2 \quad (24)$$

were

$$\phi = \frac{\pi D L \lambda_c^2 f_m^2}{c}$$

$$A_c = \frac{1}{2} E_o \{1 + e^{j\pi\gamma} J_0(m)\}$$

$$A_{ln} = A_{un} = \frac{1}{2} E_o \cdot e^{j\pi\gamma} j^n J_n(m)$$

$$A_c^* = \frac{1}{2} E_o (1 + e^{-j\pi\gamma} J_n(m))$$

$$A_{ln}^* = A_{un}^* = \frac{1}{2} E_o \cdot e^{-j\pi\gamma} (-j^n) J_n(m).$$

where  $A_{u1}$  and  $A_{l1}^*$  values are  $\frac{1}{2}E_{o1} e^{j\pi\gamma} j J_1(m) + E_{o2}$  and  $A_{u1}^* = \frac{1}{2}E_o(-j) \cdot e^{-j\pi\gamma} J_1(m) + E_{o2}$ , respectively.

To evaluate USM's performance in overcoming DPF, the calculation of C/N penalty is done using  $P_{rec}(L)$  that derived from (24). This result is then compared to the C/N penalty of the RoF channel with SD-MZM. Calculations are performed with the same parameters as previously defined. The calculations are performed for a modulation index ( $m$ ) of 1, while varying the LD<sub>2</sub> laser power at 0 dBm ( $E_{o2} = 0.045$ ), 5 dBm ( $E_{o2} = 0.08$ ) and 10 dBm ( $E_{o2} = 0.14$ ).

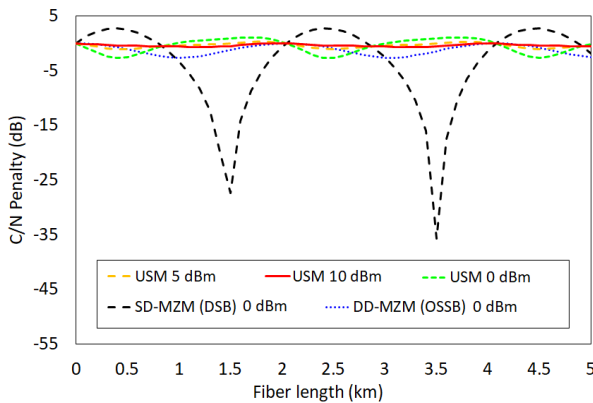


Fig. 9. C/N penalty of RoF link with SD-MZM and USM [model].

Fig. 9 shows the C/N penalty curve for both the RoF link utilizing SD-MZM and USM. From the curve it can be seen that USM can effectively handle DPF. This is characterized by the minimal power fluctuations and the absence of deep fades. The DPF levels observed for the

RoF link employing USM with LD<sub>2</sub> power set at 0, 5 and 10 dBm are recorded as 1.3, 0.4, and 0.2, respectively. This indicates that higher LD<sub>2</sub> power results in improved performance of the USM scheme. For the same  $m$ , the DPF level on the RoF channel with the OSSB spectrum generated using DD-MZM is 0.9. This means that the USM modulation scheme with LD<sub>2</sub> power of 5 and 10 dBm surpasses the performance of the OSSB spectrum in effectively eliminating DPF.

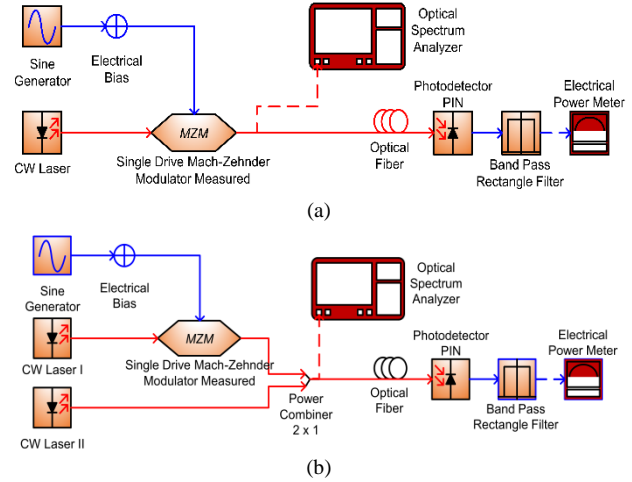


Fig. 10. RoF link simulation circuit: (a) with SD-MZM as E/O converter and (b) with USM.

#### IV. NUMERICAL SIMULATION

To validate the model and evaluate USM's performance in overcoming DPF, this study conducts simulations using the OptiSystem software. Performance evaluation is performed by comparison between the C/N penalty curves of RoF channels using SD-MZM and RoF channels using USM. The C/N penalty is obtained from the comparison of the RF signal power for various fiber lengths ( $L$ ) and RF signal power without fiber ( $L = 0$  km) which is the output of the PD.  $L$  was chosen from 0 to 5 km in 0.1 km increments. The simulation setups for both scenarios can be seen in Fig. 10. Fig 10 (a) represents the simulation circuit for the RoF channel with SD-MZM, while Fig. 10 (b) shows the simulation circuit for the RoF channel with USM.

In detail, in this research, we propose a new method to overcome DPF by changing the shape of the modulated optical spectrum from ODSB to USM. USM is generated by injecting one of the first sidebands (USB or LSB) of the ODSB signal using a second laser diode. USM can handle DPF better than DSB and OSSB by using a transmitter circuit configuration that is simpler than the OSSB transmitter circuit generated using DD-MZM. However, it should be noted that USM can overcome DPF more effectively than OSSB when LD-2 powers of 5 dBm and 10 dBm are used. The greater the LD-2 power, the more effective USM is in overcoming DPF.

The simulation circuit for RoF channel with SD-MZM comprises the following components: optical fiber, sine generator, electrical bias, photodetector PIN, CW laser,

band pass rectangle filter, SD-MZM, optical spectrum analyzer, electrical power meter, and RF spectrum analyzer. Pure RF signal ( $f_m$ ) with frequency = 60 GHz was generated using a sine generator. The switching voltage ( $V_\pi$ ) of SD-MZM is set at 2 volts. The complete settings for the SD-MZM can be seen in Table I. The sine generator voltage ( $V_m$ ) is adjusted to 0.637 V to produce a value of  $m = 1$ . The SD-MZM is fed a RF signal generated by a sine generator. To produce  $\gamma = 1/2$ , the RF signal from the sine generator is given an additional bias voltage ( $V_{bias}$ ) of 1 volt. CW laser was set with the parameters:  $\lambda_c = 193.414$  THz, linewidth = 10 MHz, and Power = 0 dBm, and then used as the input optics of the SD-MZM.

The spectrum shape of the optical signal modulated using SD-MZM was examined using an optical spectrum analyzer (OSA). The shape of the output optical signal spectrum of SD-MZM can be seen in Fig. 11 (a). The SD-MZM output is sent to receiver via single mode fiber, with fiber parameters as specified in Table II. Because this simulation is focused on observing the impact of chromatic dispersion on the power of received RF signal, the effect of fiber attenuation is disregarded. A PIN photodetector set with parameters dark current = 10 nA and Responsivity = 1 A/W is used to detect optical signals at the receiver. The output of photodetector is then filtered using a band pass rectangle filter to remove unwanted frequencies. To obtain a 60 GHz frequency of RF signal, the band pass rectangle filter parameters are configured as follows: frequency = 60 GHz, bandwidth = 10 MHz, depth = 100 dB, and insertion loss = 0 dB. The resulting RF signal power is measured using an electrical power meter. Power measurements were carried out across varying fiber lengths, ranging from 0 to 5 km with intervals of 0.1 km.

TABLE I. THE PARAMETER SETTING OF SD-MZM

Parameters	Value	Units
Splitting ratio	1.3	-
Modulation type	Phase-Shift	-
Bias Voltage 1	-4	V
Bias Voltage 2	-2	V
Normalize electrical signal	Unchecked	-
Operation mode	Change in V2 = 0	-

TABLE II. THE PARAMETER SETTING OF OPTICAL FIBER

Parameters	Value	Units
Attenuation effect	Unchecked	-
Third-rder Dispersion	Unchecked	-
Reference wavelength	193.414	THz
Length	0 – 5	Km
Group Velocity Dispersion	Checked	-
Dispersion	17	ps/nm/km

The simulation circuit for RoF link with USM has almost the same components as the simulation circuit for RoF channel with SD-MZM. But in the RoF link with USM, the output of SD-MZM is combined with the output of CW laser II using power combiner (PC). Because the  $f_m$

used is 60 GHz, the CW laser II is set with  $\lambda_c = 193.474$  THz, linewidth = 10 MHz. The power of the CW laser II is varied by 0, 5 and 10 dBm. The PC output is connected to the OSA to see the shape of the optical spectrum of the USM signal. The shape of the optical spectrum of the USM signal can be seen in Fig. 11 (b), Fig. 11 (c) and Fig. 11 (d). A single-mode optical fiber is then used to transmit the PC output. At the receiver, a PIN photodetector is used to detect optical signals. A band pass rectangle filter is used to select the RF signal with the desired frequency. The generated RF signal power is measured using an electrical power meter. Measurements were taken at fiber lengths of 0, 0.1, 0.2, ... 5 km.

Fig. 11 illustrates the profiles of the SD-MZM and USM output spectrum. The horizontal and vertical axis corresponds to frequency in Hz and the power of each component in dBm, respectively. In Fig. 11 (a), it is evident that the SD-MZM output spectrum is in the form of a double sideband, wherein the magnitude of the upper and lower sideband power for all orders are identical. The spectrum of the USM optical signal with an LD<sub>2</sub> power of 0 dBm can be seen in Fig. 11 (b). The upper and lower sideband power of order I exhibit a difference of 14 dB. Similarly, the spectrum of the USM optical signal with an LD<sub>2</sub> power of 5 dBm is illustrated Fig. 11 (c), showing a 20 dB difference in the upper and lower sideband power of order. In Fig. 11 (d), the spectrum of the USM optical signal is displayed with an LD<sub>2</sub> power of 10 dBm, wherein the upper and lower sideband powers of order I differ by 25 dB. From Fig. 11 it can be said that the derived (10) and (21) can accurately represent the optical fields of both the SD-MZM and USM outputs.

It should be noted that for additional explanation, Fig. 9 and Fig. 12, show the performance of a standard RoF system with a DSB spectrum, a RoF system with an OSSB spectrum, and a RoF system with a USM optical spectrum. These figures illustrate that the RoF system with the USM spectrum has a curve with smaller fluctuations compared to the RoF system with the OSSB spectrum. It is indicating that USM can handle DPF better than OSSB. The connection between this and DD-MZM is that the OSSB spectrum in this RoF system is generated using DD-MZM, which receives an optical signal input modulated by two RF signals with a phase difference of 90 degrees.

In details, the DPF level was evaluated by calculating the standard deviation of the C/N penalty values at all points along a 5 km length. In Fig. 9, it is shown that for a RoF system with OSSB, the DPF level is 0.9. For a RoF system with USM, with LD<sub>2</sub> power levels of 0 dBm, 5 dBm, and 10 dBm, the DPF levels are 1.3, 0.4, and 0.2, respectively. This means that USM with LD<sub>2</sub> power levels of 5 and 10 dBm has better DPF levels of 0.4 and 0.2. Meanwhile, the performance of USM with an LD<sub>2</sub> power of 0 dBm is similar to OSSB. However, it should be noted that OSSB modulation using the DD-MZM scheme requires a complex transmitter setup. Here, we propose a USM solution for eliminating dispersion without using the DD-MZM scheme.

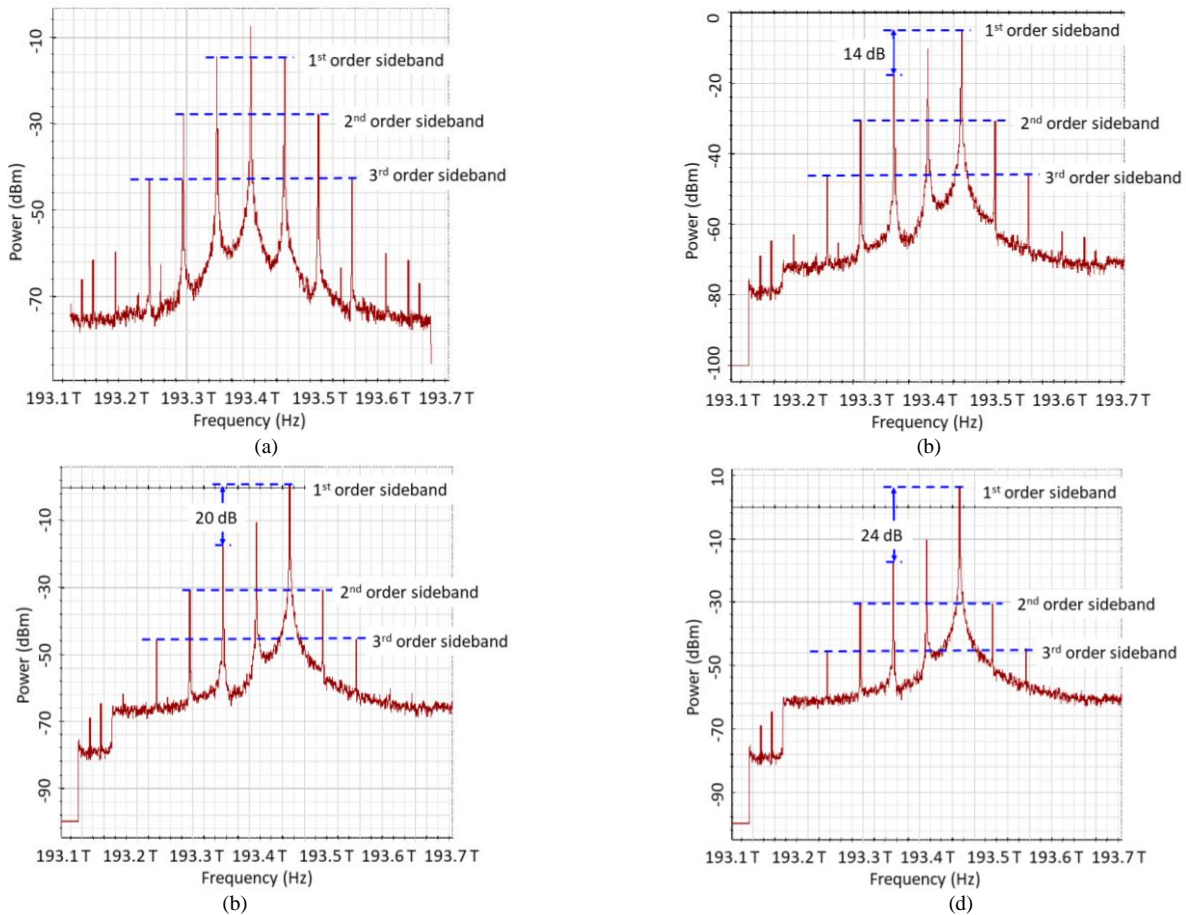


Fig. 11. The spectrum shape of (a) SD-MZM Output, (b) 0 dBm USM, (c) 5 dBm USM, and (d) 10 dBm USM RoF link simulation circuit.

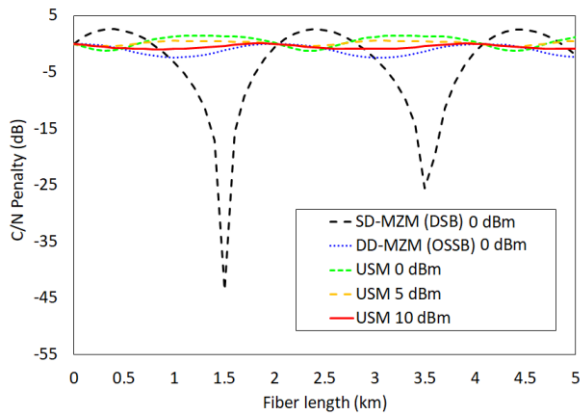


Fig. 12. C/N penalty simulation of RoF link with SD-MZM, DD-MZM, and USM.

Then, Fig. 12 depicts the C/N penalty curves derived from the simulated RoF link configurations utilizing SD-MZM and USM. These curves are constructed by computing the difference between the simulated power at a given length  $L$  and the simulated power at  $L = 0$  km. On the RoF link with SD-MZM, deep fade occurs at  $L = 1.5$  and  $L = 3.5$  km. These values of  $L$  are consistent with the results of previous calculations. Conversely, the RoF link equipped with USM experiences no deep fades. DPF level for RoF link using USM with LD<sub>2</sub> powers of 0 dBm, 5 dBm, and 10 dBm are measured at 0.9, 0.3 and 0.3. The simulation results show that the RoF link with USM at LD<sub>2</sub> powers of 5 dBm and 10 dBm, exhibits equivalent

performance. Comparing these outcomes to the calculation results, it becomes evident that the performance of the RoF link with USM is enhanced with higher LD<sub>2</sub> power levels. Moreover, it can be observed that even OSSB modulation also has a low C/N penalty value. However, implementing this DD-MZM scheme requires a complex transmitter setup.

It should be noted that, as a limitation of this study, it is shown that only laser powers of 5 dBm and 10 dBm can overcome DPF better than OSSB. This means that for LD<sub>2</sub> power greater than 10 dBm, USM performance will be better than OSSB, whereas if the laser power is smaller than 5 dBm, USM performance will be increasingly reduced. This is because the smaller the difference in USB power compared to LSB, the smaller the difference in the resulting RF<sub>1</sub> and RF<sub>2</sub> signal power will be. The lesser the magnitude of the difference, the greater the interference encountered.

A more comprehensive evaluation of the USM's performance in overcoming DPF can be observed through a detailed comparison of the calculated and simulated results, as depicted in the curves of Fig. 13. In Fig. 13 (a), Fig. 13 (b), and Fig. 13 (c), C/N penalty curves for the RoF links employing USM are presented, showing the calculated and simulated outcomes for LD<sub>2</sub> powers of 0 dBm, 5 dBm, and 10 dBm, respectively. Both model calculations and numerical simulations conclusively demonstrate that the USM method effectively mitigates DPF, offering a promising solution in optical communication networks.

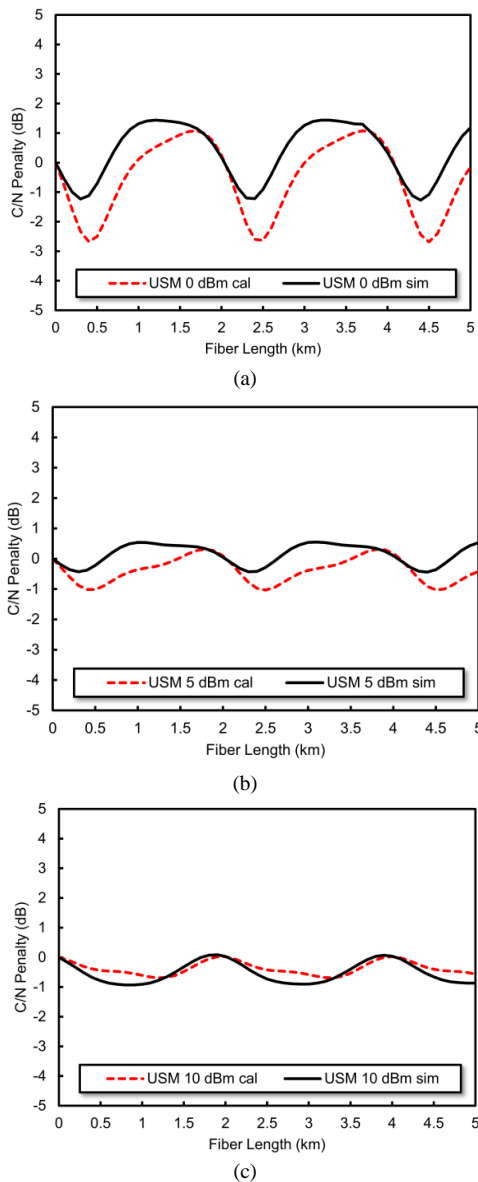


Fig. 13. The spectrum shape of (a) SD-MZM Output, (b) 0 dBm USM, (c) 5 dBm USM, and (d) 10 dBm USM RoF link simulation circuit

## V. CONCLUSION

In this study, a novel technique of USM method is successfully developed to address DPF. USM is realized by modulating the optical carrier signal with an RF signal using a SD-MZM. The output of the SD-MZM is then combined with an optical signal of a frequency equivalent to the sum of the optical carrier frequency and the RF signal frequency. The result outcomes indicate that at a modulation index ( $m$ ) of 1, the DPF level of a RoF link utilizing conventional SD-MZM as an Electro-Optic (E/O) converter is approximately 8.2. In contrast, the DPF level for a RoF link employing the OSSB modulation is around 0.9. Remarkably, the DPF level drops significantly to 0.2 when adopting the USM scheme. This result shows the highly capability of the USM scheme in eliminating DPF surpassing the performance of both the conventional SD-MZM modulation scheme and the OSSB scheme generated by DD-MZM. Then, both model calculations and numerical simulations conclusively demonstrate that

the USM method effectively mitigates DPF, offering a promising solution in optical communication systems.

## FUNDING

This research was supported by Penelitian Fundamental Reguler. DRTPM Kementerian Pendidikan, Kebudayaan, Riset, dan Teknologi. Indonesia. 2024.

## CONFLICT OF INTEREST

The authors declare no conflict of interest.

## AUTHOR CONTRIBUTIONS

Febrizal Ujang conducted the research including conceptualization, data curation, formal analysis, investigation, methodology, validation, visualization, writing the original draft, and writing for review and editing. Esra Erianti Butar Butar, Silvia Anggraeni, and Syah Alam contributed to formal analysis, investigation, methodology, and validation, as well as review and editing. Ken Paramayudha and Rocky Alfan contributed to review and editing. Teguh Firmansyah provided supervision and contributed to writing for review and editing.

## REFERENCES

- [1] D. S. Akram and H. M. Al-Tamimi, "Design of DWDM optical communication systems with different modulation formats using DCF and a repeater," *Applied Optics*, vol. 62, no. 2, pp. 429–439, 2023.
- [2] H. Yang, Y. Li, and X. Li, "Intensity-modulated refractive index sensor based on the side modes of fiber Bragg grating," *Optics Communications*, vol. 505, #127319, 2022.
- [3] D. Zou, F. Li, W. Wang, M. Yin, Q. Sui, and Z. Li, "Modified Gerchberg-Saxton algorithm based electrical dispersion pre-compensation for intensity-modulation and direct-detection systems," *Journal of Lightwave Technology*, vol. 40, no. 9, pp. 2840–2849, 2022.
- [4] K. V. Baliž and B. Batagelj, "Stabilized dispersion-robust millimeter-wave anything-over-fiber transmitter in access networks featuring a double sideband suppressed carrier modulation," in *Proc. of 2023 Int. Workshop on Fiber Optics on Access Networks*, 2023, pp. 52–56.
- [5] S. Kaur, "Performance analysis of DP-QPSK with CO-OFDM using OSSB generation," *Wireless Networks*, vol. 28, no. 4, pp. 1719–1730, 2022.
- [6] Z. Xu, M. Xue, Y. Heng, X. Zhu, and S. Pan, "Ultra-high resolution optoelectronic frequency responses measurement with doubled measurement range," in *Proc. 2021 Int. Conf. on Optical Instruments and Technology: Optoelectronic Measurement Technology and Systems*, 2022, SPIE, vol. 12282, pp. 425–430.
- [7] M. Xue, Q. Wang, Z. Xu, Y. Heng, C. Yu, and S. Pan, "Large dynamic and precision optical vector analysis assisted by SBS processing," *Journal of Lightwave Technology*, vol. 40, no. 8, pp. 2435–2440, 2022.
- [8] I. G. Insua, "Optical generation of mm-wave signals for use in broadband radio over fiber systems," *Doktoringenieurs, von der Fakult ä Elektrotechnik und Informationstechnik der, Technische Universit ä Dresden*, 2010.
- [9] C. R ős, Q. Du, Y. Zhang, *et al.*, "Ultra-compact nonvolatile phase shifter based on electrically reprogrammable transparent phase change materials," *PhotonIX*, vol. 3, no. 1, #26, 2022.
- [10] H. Yan, J. Bi, D. Guo, *et al.*, "Q-band MMW transmission enabled by joint probabilistic shaping and precoding with MZM-based OCS modulation," *IEEE Photonics Journal*, vol. 15, no. 4, pp. 1–5, 2023.
- [11] X. J. Fan, J. F. Du, G. Z. Li, M. Li, N. H. Zhu, and W. Li, "RF self-interference cancellation and frequency downconversion with immunity to power fading based on optoelectronic oscillation," *Journal of Lightwave Technology*, vol. 40, no. 12, pp. 3614–3621,

2022.

[12] Z. Zhu, C. Gao, S. Zhao *et al.*, “Filter-less photonic RF image-reject mixing with simultaneous self-interference cancellation and fiber transmission,” *Journal of Lightwave Technology*, vol. 40, no. 24, pp. 7799–7807, 2022.

[13] R. Wang, Y. Fan, J. Tan *et al.*, “A linearized optical single-sideband modulation RoF link with tunable optical carrier-to-sideband ratio,” *Optics Communications*, vol. 511, #127991, 2022.

[14] Y. Li, J. Yu, R. Song, and N. Liu, “D-band signal generation and transmission without optical filter based on optical carrier suppression and single-sideband modulation,” *Optics Express*, vol. 30, no. 1, pp. 436–446, 2022.

[15] R. Garg, G. Kaur, and N. Kumar, “Performance analysis of  $2\lambda \times 160$  Gbps optical single sideband (OSSB) generation in polarization division multiplexed (PDM) QPSK based satellite wireless optical systems (SWOS),” *Journal of Optical Communications*, vol. 28, no. 4, pp. 1719–1730, 2022.

[16] P. Xia, H. Yu, Z. Wei *et al.*, “Single chip silicon single sideband modulator with high sideband suppression ratio,” in *Proc. AOPC 2022: Optoelectronics and Nanophotonics*, 2023, SPIE, vol. 12556, pp. 148–151.

[17] C. Yi, Y. Zhao, W. Zhuang, J. Chen, T. Shi, and X. Qin, “Optical single-sideband (OSSB) Raman laser system based on an atomic filter for atom gravimeters,” *Optics Letters*, vol. 49, no. 10, pp. 2745–2748, 2024.

[18] Z. Chen, Y. Luo, and H. Zou, “High-resolution optical vector analysis based on single sideband modulation using a dual port Mach–Zehnder modulator,” *Optical Engineering*, vol. 63, no. 3, pp. 038103–038103, 2024.

[19] N. Singh, G. Torfs, J. Van Kerrebrouck, R. Broucke, P. Demeester, and X. Yin, “60 GHz analog radio-over-fiber single sideband transmitter chipset with 55nm SiGe BiCMOS driver RFIC and silicon photonics modulator PIC,” *Journal of Lightwave Technology*, vol. 41, no. 11, pp. 3620–3627, 2023.

[20] B. Mallick, P. Parida, C. Nayak *et al.*, “Long distance QKD propagation using optical single sideband scheme,” *Optics Continuum*, vol. 3, no. 3, pp. 427–440, 2024.

[21] Y. Zhou, J. Xiao, C. Zhao, J. Zuo, J. Ming, and L. Zhao, “Simplified twin-single-sideband direct detection system separating left and right sideband signals using a digital signal processing algorithm instead of optical bandpass filters,” *Optics Express*, vol. 30, no. 1, pp. 619–628, 2022.

[22] A. A. Júnior, J. A. Ribeiro, and D. H. Spadoti, “Large signal analysis on microwave photonic generation using an asymmetric dual-drive Mach–Zehnder modulator and with different modulation indices,” *Microwave and Optical Technology Letters*, vol. 64, no. 7, pp. 1176–1184, 2022.

[23] P. Kumar, M. D. Nadeem, R. Raj, S. K. Raghuvanshi, and S. Kumar, “Advancing microwave signal generation: frequency quadrupling using dual-drive Mach-Zehnder modulator,” *Integrated Optics: Devices, Materials, and Technologies XXVIII*, 2024, SPIE, vol. 12889, pp. 124–130.

[24] J. Ming, J. Xiao, J. Song *et al.*, “Synthesis of MSBS-32QAM in a DD-MZM based simplified twin-SSB system via IM/DD,” *Journal of Lightwave Technology*, vol. 42, no. 8, pp. 2683–2692, 2023.

[25] W. Wang, Y. Bai, S. Fu *et al.*, “High linearity microwave photonic up-conversion system based on parallel dual-drive Mach–Zehnder modulators,” *Photonics*, vol. 9, no. 4, #236, 2022.

[26] X. Tang, M. Ding, Y. Xiao *et al.*, “Programmable optical digital logic computing array using dual-drive Mach-Zehnder modulators,” *IEEE Journal of Selected Topics in Quantum Electronics*, vol. 30, no. 3, pp. 267–277, 2023.

[27] B. Tamrakar, K. Singh, and P. Kumar, “Analysis and Modelling of DD-DPMZM to Investigate Fundamental to Intermodulation Distortion Ratio (FIMDR) Against Different Fiber Impairments for the Next Generation Networks,” *Journal of Active & Passive Electronic Devices*, vol. 16, no. 4, pp. 297–310, 2022.

[28] V. A. Thomas, M. El-Hajjar, and L. Hanzo, “Performance improvement and cost reduction techniques for radio over fiber communications,” *IEEE Communications Surveys & Tutorials*, vol. 17, no. 2, pp. 627–670, 2015.

[29] D. Colton and R. Kress, *Inverse Acoustic and Electromagnetic Scattering Theory*, 3rd ed. Springer Science & Business Media, 1998, p. 406.

[30] F. Ujang, T. Firmansyah, P. S. Priambodo, and G. Wibisono, “Irregular shifting of RF driving signal phase to overcome

dispersion power fading,” *Photonics*, vol. 6, no. 4, #104, 2019.

[31] R. J. Davies, “Optical single sideband for broadband and subcarrier systems,” Dissertation, Department of Electrical and Computer Engineering, University of Alberta, 1999.

[32] G. Meslener, “Chromatic dispersion induced distortion of modulated monochromatic light employing direct detection,” *IEEE Journal of Quantum Electronics*, vol. 20, no. 10, pp. 1208–1216, 1984.

Copyright © 2024 by the authors. This is an open access article distributed under the Creative Commons Attribution License (CC BY-NC-ND 4.0), which permits use, distribution and reproduction in any medium, provided that the article is properly cited, the use is non-commercial and no modifications or adaptations are made.



**Febrizal Ujang** was born in Selatpanjang, Indonesia. He received B.Eng (S.T) degree in electrical engineering from Universitas Sumatera Utara, Indonesia in 2002, and M.Eng (M.T) degree in telecommunication engineering from Institut Teknologi Bandung, Indonesia in 2009. He joined the Department of Electrical Engineering Universitas Riau as a researcher and lecturer. He received Ph.D. degree in electrical engineering at Department of Universitas Indonesia in 2021. His research interests include coding and wireless communications, electronics and optical communications.



**Anhar** has been a lecturer at the University of Riau since 2002. He took his PhD level at Brunel University London, and graduated in 2019. Currently, he is a senior lecturer and has been teaching many subjects such Data communication, Traffic Engineering, Wireless Sensor Networks, Electrical Measurement, and signals and systems. In terms of research, he has been supervising many students and publishing many articles related to the network performance analysis. He is also interesting to investigate the performance of Medium Access Control (MAC) and routing protocols in sensor networks, Internet of Things (IoT), and Wifi.



**Esra Erianti Butar Butar** was born on April 26<sup>th</sup>, 2001 in Pekanbaru, Indonesia. Currently studying for a Bachelor of Electrical Engineering at the Universitas Riau, Indonesia in the field of telecommunications. In 2023, she made a journal about the performance comparison of radio frequency level multiplexing and optical level multiplexing in radio systems over fiber.



**Silvia Anggraeni** has been a lecturer at Department of Electrical Engineering Universitas Pembangunan Nasional Veteran Jakarta since 2021. She received a bachelor's degree of electrical engineering from Universitas Indonesia in 2001. She took her Master at Universiti Teknologi Petronas, Malaysia then earned her PhD at the same university in 2018. Her research interests include channel coding, communication systems, circuit design, data and

computer networks



**Syah Alam** was born in Jakarta, Indonesia. He received Bachelor Education of Engineering (S.Pd) degree in electrical engineering from Universitas Pendidikan Indonesia (UPI) and M.Eng (M.T) degree in telecommunication engineering from Graduate Programe of Electrical Engineering Universitas Trisakti in 2010 and 2012, respectively. In 2018, he joined the Department of Electrical Engineering

Universitas Trisakti as a researcher and lecturer. In 2021, he is pursuing his PhD at Universiti Teknikal Melaka Malaysia (UTeM) in the field of Electronic Engineering (RF and Microwave). His research interests include microstrip antenna, and microwave sensor for various



**Ken Paramayudha** received the B.E. degree in electrical engineering from the Bandung Institute of Technology, Indonesia, in 2009, and the M.Phil. degree in electrical and electronic engineering from the University of Adelaide, Australia, in 2019. Since 2014, he has been working as a Research Associate with the Research Center for Electronics and Telecommunication, Indonesian Institute of Sciences (PPET-LIPI). In 2017, he received the

Riset-PRO Scholarship from the Indonesian Ministry of Research, Technology, and Higher Degree Education to continue his master's study with the University of Adelaide. He joined the School of Electrical and Electronic Engineering as a research student in the area of applied electromagnetics. His current research interests include reconfigurable antennas and microwave devices. During his candidature, he was the finalist of the Best Student Paper Award at Australian Microwave Symposium in 2018. He was a recipient of the Best Poster Presentation Award at Indonesia–Japan Workshop on Antennas and Wireless Technology in 2019



**Rocky Alfanz** was born in Jakarta, Indonesia. He is a lecturer at Sultan Ageng Tirtayasa University's Department of Electrical Engineering since 2010. He Received a bachelor's degree (S.T) in electrical engineering from Jayabaya University in Jakarta, Indonesia (2007). Earned a doctoral degree (Dr. Eng.) from Kumamoto University, Japan (2020) after completing the Master's program (M.Sc.) at National Taiwan University, Taiwan (2009). In

addition, he oversees the quality and photovoltaic module sensor instruments laboratory at Sultan Ageng Tirtayasa University's Faculty of Engineering. He has more than 100 articles published in journal and conference and frequently speaks at national conferences on renewable energy. His research interests include photovoltaics module system and instrument sensor devices for various applications and he owns the rights to distribute Japanese solar cell products in Indonesia.



**Teguh Firmansyah** was born in Subang, Indonesia. He received the B.Eng. (S.T.) degree in electrical engineering and the M.Eng. (M.T.) degree in telecommunication engineering from the Department of Electrical Engineering, Universitas Indonesia, in 2010 and 2012, respectively. He received the Ph.D. degree (Dr. Eng) from Shizuoka University Japan in 2022. In 2012, he joined the Department of Electrical Engineering, Universitas Sultan Ageng

Tirtayasa, as a Lecturer. He has authored or coauthored over 40 articles published in refereed journals and conferences. He holds two patents for wideband antenna and multiband antenna. His research interests include microstrip antenna and microwave circuit for various applications. He is a member of the IEEE Antenna and Propagation Society and the IEEE Microwave Theory and Technique Society. He has been a Reviewer of Electronics Letters, the International Journal of Microwave and Wireless Technologies (Cambridge), Wireless Personal Communications (Springer), the International Journal of Electronics and Communications (Elsevier), Microwave and Optical Technology Letters (Wiley), the International Journal of RF and Microwave Computer-Aided Engineering (Wiley), IEEE Access, and IEEE Sensors Journal.